Exploring acoustic wave transmission in micropolar plate in air

Christian Meso, Hervé Franklin, Erick Ogam, Zine El Abiddine Fellah

▶ **To cite this version:**

Christian Meso, Hervé Franklin, Erick Ogam, Zine El Abiddine Fellah. Exploring acoustic wave transmission in micropolar plate in air. 53rd International Congress & Exposition on Noise Control Engineering, Aug 2024, Nantes, France. hal-04695277

HAL Id: hal-04695277
https://hal.science/hal-04695277

Submitted on 12 Sep 2024

HAL is a multi-disciplinary open access archive for the deposit and dissemination of scientific research documents, whether they are published or not. The documents may come from teaching and research institutions in France or abroad, or from public or private research centers.

L'archive ouverte pluridisciplinaire **HAL**, est destinée au dépôt et à la diffusion de documents scientifiques de niveau recherche, publiés ou non, émanant des établissements d'enseignement et de recherche français ou étrangers, des laboratoires publics ou privés.

Exploring acoustic wave transmission in micropolar plate in air

Meso Christian[1]
Aix Marseille Univ, CNRS, Centrale Marseille, LMA UMR 7031, Marseille, France

Franklin Hervé[2]
Laboratoire Ondes et Milieux Complexes LOMC UMR CNRS 6294, 75 rue Bellot, Université Le Havre Normandie, Le Havre, France

Ogam Erick[3]
Aix Marseille Univ, CNRS, Centrale Marseille, LMA UMR 7031, Marseille, France

Fellah Zine El Abbidine[4]
Aix Marseille Univ, CNRS, Centrale Marseille, LMA UMR 7031, Marseille, France

ABSTRACT

This study explores the behavior of sound wave propagation across a micropolar plate at diverse incident angles, specifically crafted from expanded polystyrene. Through a blend of theoretical formulations and practical experimentation, we scrutinize the alterations in transmission coefficients within the frequency spectrum, shedding light on the dynamic shifts in various vibrational modes. Utilizing a comprehensive setup comprising a loudspeaker, microphone, and National Instruments acquisition system, we meticulously discerned the initial trio of longitudinal vibration modes across a broad frequency span extending up to $70kHz$*. Notably, despite the plate's inherent dispersion and attenuation traits, this experimental setup proved effective. A distinctive facet of our approach lies in the deliberate incorporation of multiple incident angles, which yielded crucial insights. Notable is the identification, within the experiments, of a critical angle* θ_{cr}*, marking a transitional zone. Below this threshold, distinct Lamb modes dominate, while beyond it, the emergence of micropolar modes becomes apparent. These empirically validated findings, in alignment with theoretical projections, substantially enrich our comprehension of these materials' engineering applications.*

1. INTRODUCTION

In 1909, the Cosserat brothers, Eugène and François, introduced a variant of continuum mechanics, paving the way for models of polar continua that incorporate stress couples [1]. This development led to the linear theory of polar continua, known as the mechanics of micropolar continua, which accounts for microinertial effects [2–11]. Our focus in this study lies specifically on linear elastic media with micropolar characteristics, where deformations are reversible under the influence of microscale phenomena. This entails assigning a general intrinsic deformation to each material point, augmenting the classical translational degree of freedom with six additional ones, thus characterizing the medium as micromorphic according to Eringen's classification. Assuming the microstructure's rigidity, we refer to it as a micropolar medium.The objective of our research is to investigate acoustic transmission properties through a linear micropolar elastic plate in air and examine resulting vibration modes. To achieve this, we derive transmission and reflection coefficients to generalize expressions previously formulated for plates in classical

[1]meso@lma.cnrs-mrs.fr

[2]herve.franklin@univ-lehavre.fr

[3]ogam@lma.cnrs-mrs.fr

[4]fellah@lma.cnrs-mrs.fr

Permission is granted for the reproduction of a fractional part of this paper published in the Proceedings of INTER-NOISE 2024 provided permission is obtained from the author(s) and credit is given to the author(s) and these proceedings.

elasticity by Viktorov [12] and later elaborated by Fiorito, Madigosky, and Uberall [13, 14]. Their work formalized these expressions and provided clear interpretations of transmission and reflection coefficients. A similar formalism, albeit excluding resonance considerations, may prove valuable for leveraging the S-matrix method [15] and comprehensively interpreting generalized Lamb modes.

This paper enriches the field of micropolar mechanics by experimentally validating the existence of Lamb and micropolar modes, which supports theoretical models describing how isotropic, linear, elastic media react to acoustic waves. We introduce the governing equations for wave propagation in a micropolar elastic medium in air in Section 2. This includes a detailed mathematical expression of the transmission coefficient, alongside a case-specific analysis using numerical simulations provided by Ogam et al. [16] in Section 3. By adjusting the incidence angle, we investigate the emergence of micropolar modes beyond a certain threshold. The subsequent sections, 4 and 5, outline our experimental approach and showcase findings that confirm the theoretical predictions, bridging theory with experimental evidence.

2. WAVES PROPAGATION IN THE MICROPOLAR ELASTIC MEDIA

The section explores the complex dynamics of wave propagation through micropolar elastic materials. Our objective is to investigate very briefly, how acoustic waves behave in these media, uncovering the fundamental principles that govern their propagation and revealing their distinctive characteristics.

Through this exploration, we gain valuable insights into the intricate relationship between micropolar properties and wave phenomena, advancing our comprehension of elastic wave propagation within these materials.

2.1. Phases velocities

Predictions by Parfitt and Eringen [9, 17] for such a medium anticipated a response characterized by the propagation of four harmonic plane waves, each with distinct phase velocities depending upon the angular frequency ω. These waves include :

- A longitudinal displacement wave at velocity $v_1(\omega)$,
- A longitudinal micro-rotation wave at velocity $v_2(\omega)$, featuring microrotation aligned with the direction of propagation, and
- Two transverse displacement coupled to microrotation waves, each with velocities $v_3(\omega)$ and $v_4(\omega)$ respectively.

The expressions for these different velocities can be written in the following form :

$$v_1^2 = \frac{\lambda + 2\mu + K}{\rho} \tag{1}$$

$$v_2^2 = \frac{\alpha + \beta + \gamma}{\rho J\left(1 - \frac{\omega_0^2}{\omega^2}\right)} \tag{2}$$

$$v_3^2 = \frac{\omega^2}{\frac{1}{2}\left(1+\frac{\mu+K}{\gamma}\right)\frac{\omega^2}{(\mu+K)} - \left(1-\frac{J\omega_0^2}{4(\mu+K)}\right)\frac{\omega_0^2}{2\gamma} - \sqrt{\left[\frac{1}{2}\left(1+\frac{\mu+K}{\gamma}\right)\frac{\omega^2}{(\mu+K)} - \left(1-\frac{J\omega_0^2}{4(\mu+K)}\right)\frac{\omega_0^2}{2\gamma}\right]^2 - \frac{\omega^2(\omega^2-\omega_0^2)}{(\mu+K)\gamma}}} \tag{3}$$

$$v_4^2 = \frac{\omega^2}{\frac{1}{2}\left(1+\frac{\mu+K}{\gamma}\right)\frac{\omega^2}{(\mu+K)} - \left(1-\frac{J\omega_0^2}{4(\mu+K)}\right)\frac{\omega_0^2}{2\gamma} + \sqrt{\left[\frac{1}{2}\left(1+\frac{\mu+K}{\gamma}\right)\frac{\omega^2}{(\mu+K)} - \left(1-\frac{J\omega_0^2}{4(\mu+K)}\right)\frac{\omega_0^2}{2\gamma}\right]^2 - \frac{\omega^2(\omega^2-\omega_0^2)}{(\mu+K)\gamma}}} \tag{4}$$

Equations (1), (2), (3), and (4) involve several parameters. The mass density of the medium is denoted by ρ. The symbols λ and μ represent Lamé moduli, while K corresponds to Cosserat's

couple modulus, which characterizes the micropolar state. The quantities α, β, and γ stand for rotational micro-inertia constants. Dividing them by the microinertia constant J yields moduli, with γ often referred to as the twist coefficient. Additionally, ω_0^2 is defined as $\frac{2K}{\rho J}$.

Singh and Kumar [18] conducted a comprehensive study on the reflection and transmission of elastic waves at interfaces involving micropolar elastic half-spaces, while Parfitt and Eringen [17] delved into the reflection phenomena of elastic plane waves [19] from flat boundaries of such media.

2.2. Analysis of the elastic behavior of a micropolar plate

Let's explore the intricate dynamics of how a micropolar plate reacts to external forces and stimuli. Through an examination of the plate's elastic behavior, our goal is to reveal the fundamental principles that govern its mechanical response.

Let's start by mathematically modeling a plate with a thickness of $2h$ and subject to the constitutive equations of linear isotropic micropolar elasticity. This plate is in contact with air through its outer faces Γ_a and Γ_b, as illustrated in Figure 1. The angles of incidence and transmission are denoted by θ_a and θ_b, respectively.

Introducing scalar displacement potentials ψ_a for the air on the Γ_a side and ψ_b for the Γ_b side, we describe the displacement and pressure on both sides, the expressions for which are given in Equations 5 and 6. On Γ_a, the displacement in the z-direction and pressure are represented by $u_{az} = \partial\psi_a/\partial z$ and $P_a = -\rho_a\partial^2\psi_a/\partial t^2$, respectively. Similarly, for Γ_b, we have $u_{bz} = \partial\psi_b/\partial z$ and $P_b = -\rho_b\partial^2\psi_b/\partial t^2$. Here, ∂ denotes differentiation with respect to either the spatial coordinate z or time t. Inside the plate, we introduce $q(y,z,t)$ as a scalar potential function, and Π_x, Θ_y, and Θ_z as the respective components of vector potential functions.

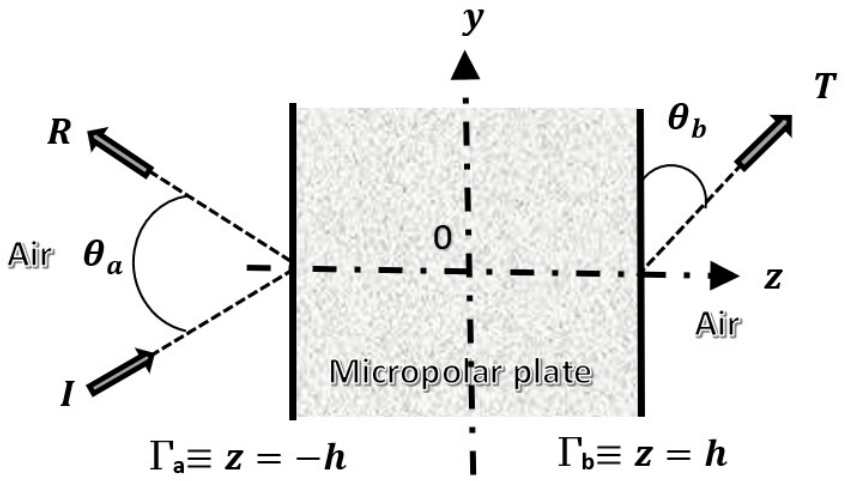

Figure 1: The geometry of the problem under oblique incidence

$$\psi_a = A_{aI}e^{ik_{az}z}e(y,t) + A_{aR}e^{-ik_{az}z}e(y,t) \tag{5}$$

$$\psi_b = A_{bT}e^{ik_{bz}z}e(y,t) \tag{6}$$

where

$$e(y,t) = e^{i\left(\frac{\omega}{c_a}\sin\theta_a y - \omega t\right)} = e^{i\left(\frac{\omega}{c_b}\sin\theta_b y - \omega t\right)}, \tag{7}$$

$$k_{az} = \frac{\omega}{c_a}\cos\theta_a, \quad k_{bz} = \frac{\omega}{c_b}\cos\theta_b, \tag{8}$$

$$k_y = k_a\sin\theta_a = k_b\sin\theta_b, \tag{9}$$

and the velocities in the fluids in general on the Γ_a and Γ_b sides are represented by c_a and c_b, respectively.

Let's define $q \equiv q(y,z,t)$ as the scalar potential displacement in the plate. The components of interest in our analysis are those of the stress tensor σ and the couple stress tensor m. It's worth noting the comparison with Eqs. (5.17.2) in the reference [9], where $\bar{U}$ and $\bar{\phi}$ are employed instead of Π_x and $\Theta_{z,y} - \Theta_{y,z}$ respectively. However, it's important to highlight that this substitution does not lead to an exact interpretation of plate vibration modes as observed in vacuum.

$$\sigma_{zz} = (q_{,zz} - \Pi_{x,zy})(2\mu + K) + \nabla^2 q\lambda \tag{10}$$

$$\sigma_{zy} = -K(\Theta_{y,z} - \Theta_{z,y}) + q_{,yz}(K + 2\mu) + (\mu + K)\Pi_{x,zz} - (\Pi_{x,yy})\mu, \tag{11}$$

$$m_{zx} = -\gamma\Theta_{y,zz} + \gamma\Theta_{z,zy} \tag{12}$$

Below are expansions that could be considered for the aforementioned quantities :

$$q = [(a_1\cos(k_{1z}z) + b_1\sin(k_{1z}z)]\, e^{i\left(\frac{\omega}{c_a}\sin\theta_a y - \omega t\right)} \tag{13}$$

$$\Pi_x = [A_3\cos(k_{3z}z) + B_3\sin(k_{3z}z) + A_4\cos(k_{4z}z) + B_4\sin(k_{4z}z)]\, e^{i\left(\frac{\omega}{c_a}\sin\theta_a y - \omega t\right)} \tag{14}$$

$$\Theta_y = \left\{\eta_{3y}\left[A_3\cos(k_{3z}z) + B_3\sin(k_{3z}z)\right] + \eta_{4y}\left[A_4\cos(k_{4z}z) + B_4\sin(k_{4z}z)\right]\right\} e^{i\left(\frac{\omega}{c_a}\sin\theta_a y - \omega t\right)} \tag{15}$$

and

$$\Theta_z = \left\{\eta_{3z}\left[A_3\cos(k_{3z}z) + B_3\sin(k_{3z}z)\right] + \eta_{4z}\left[A_4\cos(k_{4z}z) + B_4\sin(k_{4z}z)\right]\right\} e^{i\left(\frac{\omega}{c_a}\sin\theta_a y - \omega t\right)} \tag{16}$$

In the preceding equations, we can generalize the expressions for η along the y and z axes with various wave numbers, and present them as follows (with $p = 1,3,4$) :

$$\eta_{py} = \frac{-i\omega_0^2}{2\left(\frac{\omega}{v_p}\right)^2\left[v_p^2 - \frac{\omega_0^2}{\left(\frac{\omega}{v_p}\right)^2} - c_4^2\right]}\left[\left(\frac{\omega}{v_p}\right)^2 - k_y^2\right] \tag{17}$$

$$\eta_{pz} = \frac{i\omega_0^2}{2\left(\frac{\omega}{v_p}\right)^2\left[v_p^2 - \frac{\omega_0^2}{\left(\frac{\omega}{v_p}\right)^2} - c_4^2\right]}k_y \tag{18}$$

To streamline the notation and enhance clarity, it's advantageous to introduce terms denoted by Π_{px}, which encapsulate a specific combination of the incident and reflected waves propagating within the plate. This approach not only simplifies the mathematical expressions but also provides a more intuitive understanding of the wave dynamics involved.

At this point, the attention should shift to the determination of the unknown amplitudes A_{aR} and A_{bT}, while A_{aI} remains predefined. These amplitudes represent the incident (I), transmitted (T), and reflected (R) signals, respectively.

3. ANALYSIS OF THE THEORETICAL TRANSMISSION COEFFICIENT AT OBLIQUE INCIDENCE

In this section, the focus will be on establishing a comprehensive understanding of how oblique incidence influences the transmission efficiency through theoretical frameworks.

3.1. Analytical expression

To achieve this, our approach involves incorporating the boundary conditions Γ_a and Γ_b into the relationships established in Section 2. These boundary conditions, encompass four key aspects : $\sigma_{zy} = 0$, $\sigma_{zz} = -P_p$, $u_z = u_{pz}$, and $m_{zx} = 0$. Taking into account the condition $m_{zx} = 0$ at the boundaries $z = +h$ and $z = -h$, we can find the following expressions :

$$\sum_{p=3}^{4} k_{pz}^2 \eta_{py} \Pi_{px}^{+}(h) + \sum_{p=3}^{4} \left[i k_y \eta_{pz} k_{pz} \cot(k_{pz} h) \right] \Pi_{px}^{-}(h) = 0 \tag{19}$$

$$\sum_{p=3}^{4} k_{pz}^2 \eta_{py} \Pi_{px}^{-}(h) - \sum_{p=3}^{4} \left[i k_y \eta_{pz} k_{pz} \tan(k_{pz} h) \right] \Pi_{px}^{+}(h) = 0 \tag{20}$$

Analyzing the initial set of boundary conditions at Γ_a, the equations yield the following expressions upon calculation :

$$\begin{aligned} \sum_{p=3}^{4} \left(E_{aAp}^{-} - i \frac{\rho_a k_{1z}}{\rho k_{az}} \frac{2\mu + K}{\mu + K} k_y \frac{\omega^2}{c_2^2} \mathfrak{u}_p \right) \Pi_{px}^{+} + \sum_{p=3}^{4} \left(E_{aSp}^{-} + i \frac{\rho_a k_{1z}}{\rho k_{az}} \frac{2\mu + K}{\mu + K} k_y \frac{\omega^2}{c_2^2} \mathfrak{u}_p \right) \Pi_{px}^{-} \\ + 2i \frac{\rho_a k_{1z}}{\rho} \left(\frac{2\mu + K}{\mu + K} k_y \right) \left(\frac{\omega^2}{c_2^2} \right) \psi_{aI} = 0 \end{aligned} \tag{21}$$

and

$$\begin{aligned} \sum_{p=3}^{4} \left(E_{aAp}^{+} + i \frac{\rho_a k_{1z}}{\rho k_{az}} \frac{2\mu + K}{\mu + K} k_y \frac{\omega^2}{c_2^2} \mathfrak{u}_p \right) \Pi_{px}^{+} + \sum_{p=3}^{4} \left(E_{aSp}^{+} - i \frac{\rho_a k_{1z}}{\rho k_{az}} \frac{2\mu + K}{\mu + K} k_y \frac{\omega^2}{c_2^2} \mathfrak{u}_p \right) \Pi_{px}^{-} \\ + 2i \frac{\rho_a k_{1z}}{\rho} \left(\frac{2\mu + K}{\mu + K} k_y \right) \left(\frac{\omega^2}{c_2^2} \right) \psi_{aR} = 0 \end{aligned} \tag{22}$$

where :

$$\mathfrak{u}_p = \frac{\Sigma_p (\mu + K)}{(2\mu + K) k_y} - k_y \quad (p = 3, 4) \tag{23}$$

$$E_{aSp}^{+} = -\mathfrak{Z}_{aAp}^{++} k_{pz} \cot(k_{pz} h) + \left[\frac{(2\mu + K)}{\mu + K} k_y^2 - \frac{\omega^2}{c_2^2} \right] \Sigma_p \cot(k_{1z} h) \tag{24}$$

$$E_{aAp}^{-} = \mathfrak{Z}_{aSp}^{--} k_{pz} \tan(k_{pz} h) + \left[\frac{(2\mu + K)}{\mu + K} k_y^2 - \frac{\omega^2}{c_2^2} \right] \Sigma_p \tan(k_{1z} h) \tag{25}$$

$$E_{aSp}^{-} = -\mathfrak{Z}_{aAp}^{+-} k_{pz} \cot(k_{pz} h) + \left[\frac{(2\mu + K)}{\mu + K} k_y^2 - \frac{\omega^2}{c_2^2} \right] \Sigma_p \cot(k_{1z} h) \tag{26}$$

In the preceding expressions, terms Σ_p, $\mathfrak{Z}_{aSp}^{-+}$, $\mathfrak{Z}_{aAp}^{++}$, $\mathfrak{Z}_{aSp}^{--}$, and $\mathfrak{Z}_{aAp}^{+-}$ have been introduced for the sake of simplification. Subsequently, upon calculation by identification, their expressions are as follows :

$$\Sigma_p = \left(2 - \frac{K}{\mu + K} \right) k_y^2 - \frac{\omega^2}{v_p^2} + i k_y \frac{K}{\mu + K} \eta_{pz}) \quad (p = 3, 4) \tag{27}$$

$$\mathfrak{Z}_{aSp}^{-+} = \left[\frac{(2\mu + K)}{\mu + K} k_y^2 - \frac{\omega^2}{c_2^2} \right] K \eta_{py} \cot(k_{1z} h) - i \left[i \left(\frac{2\mu + K}{\mu + K} k_y \right)^2 k_{1z} + \frac{\rho_a k_{1z}}{\rho k_{az}} \frac{\omega^2}{c_2^2} K \eta_{py} \right] \tag{28}$$

$$\mathfrak{Z}_{aAp}^{++} = \left[\frac{(2\mu + K)}{\mu + K} k_y^2 - \frac{\omega^2}{c_2^2} \right] K \eta_{py} \tan(k_{1z} h) + i \left[i \left(\frac{2\mu + K}{\mu + K} k_y \right)^2 k_{1z} + \frac{\rho_a k_{1z}}{\rho k_{az}} \frac{\omega^2}{c_2^2} K \eta_{py} \right] \tag{29}$$

$$\Im_{aSp}^{--} = \left[\frac{(2\mu+K)}{\mu+K}k_y^2 - \frac{\omega^2}{c_2^2}\right] K\eta_{py}\cot(k_{1z}h) - i\left[i\left(\frac{2\mu+K}{\mu+K}k_y\right)^2 k_{1z} - \frac{\rho_a k_{1z}}{\rho k_{az}}\frac{\omega^2}{c_2^2}K\eta_{py}\right] \tag{30}$$

$$\Im_{aAp}^{+-} = \left[\frac{(2\mu+K)}{\mu+K}k_y^2 - \frac{\omega^2}{c_2^2}\right] K\eta_{py}\tan(k_{1z}h) + i\left[i\left(\frac{2\mu+K}{\mu+K}k_y\right)^2 k_{1z} - \frac{\rho_a k_{1z}}{\rho k_{az}}\frac{\omega^2}{c_2^2}K\eta_{py}\right] \tag{31}$$

Using the same reasoning at boundary Γ_b, these equations yield the following expressions upon calculation :

$$\begin{aligned}\sum_{p=3}^{4}\left(E_{bAp}^{-} + i\frac{\rho_b k_{1z}}{\rho k_{bz}}\frac{2\mu+K}{\mu+K}k_y\frac{\omega^2}{c_2^2}\mathfrak{u}_p\right)\Pi_{px}^{+} - \sum_{p=3}^{4}\left(E_{bSp}^{-} - i\frac{\rho_b k_{1z}}{\rho k_{bz}}\frac{2\mu+K}{\mu+K}k_y\frac{\omega^2}{c_2^2}\mathfrak{u}_p\right)\Pi_{px}^{-} \\ -2i\frac{\rho_b k_{1z}}{\rho}\left(\frac{2\mu+K}{\mu+K}k_y\right)\left(\frac{\omega^2}{c_2^2}\right)\psi_{bT} = 0\end{aligned} \tag{32}$$

and

$$\sum_{p=3}^{4}\left(E_{bAp}^{+} - i\frac{\rho_b k_{1z}}{\rho k_{bz}}\frac{2\mu+K}{\mu+K}k_y\frac{\omega^2}{c_2^2}\mathfrak{u}_p\right)\Pi_{px}^{+} - \sum_{p=3}^{4}\left(E_{bSp}^{+} + i\frac{\rho_b k_{1z}}{\rho k_{bz}}\frac{2\mu+K}{\mu+K}k_y\frac{\omega^2}{c_2^2}\mathfrak{u}_p\right)\Pi_{px}^{-} = 0 \tag{33}$$

$$E_{aAp}^{+} = -\Im_{bSp}^{++}k_{pz}\tan(k_{pz}h) + \left[\frac{(2\mu+K)}{\mu+K}k_y^2 - \frac{\omega^2}{c_2^2}\right]\Sigma_p\tan(k_{1z}h) \tag{34}$$

$$E_{bSp}^{+} = \Im_{bAp}^{-+}k_{pz}\cot(k_{pz}h) + \left[\frac{(2\mu+K)}{\mu+K}k_y^2 - \frac{\omega^2}{c_2^2}\right]\Sigma_p\cot(k_{1z}h) \tag{35}$$

$$E_{aAp}^{-} = -\Im_{bSp}^{+-}k_{pz}\tan(k_{pz}h) + \left[\frac{(2\mu+K)}{\mu+K}k_y^2 - \frac{\omega^2}{c_2^2}\right]\Sigma_p\tan(k_{1z}h) \tag{36}$$

$$E_{bSp}^{-} = \Im_{bAp}^{--}k_{pz}\cot(k_{pz}h) + \left[\frac{(2\mu+K)}{\mu+K}k_y^2 - \frac{\omega^2}{c_2^2}\right]\Sigma_p\cot(k_{1z}h) \tag{37}$$

where

$$\Im_{bSp}^{+-} = \left[\frac{(2\mu+K)}{\mu+K}k_y^2 - \frac{\omega^2}{c_2^2}\right] K\eta_{py}\cot(k_{1z}h) + i\left[i\left(\frac{2\mu+K}{\mu+K}k_y\right)^2 k_{1z} + \frac{\rho_b k_{1z}}{\rho k_{bz}}\frac{\omega^2}{c_2^2}K\eta_{py}\right] \tag{38}$$

$$\Im_{bAp}^{--} = \left[\frac{(2\mu+K)}{\mu+K}k_y^2 - \frac{\omega^2}{c_2^2}\right] K\eta_{py}\tan(k_{1z}h) - i\left[i\left(\frac{2\mu+K}{\mu+K}k_y\right)^2 k_{1z} + \frac{\rho_b k_{1z}}{\rho k_{bz}}\frac{\omega^2}{c_2^2}K\eta_{py}\right] \tag{39}$$

$$\Im_{bSp}^{++} = \left[\frac{(2\mu+K)}{\mu+K}k_y^2 - \frac{\omega^2}{c_2^2}\right] K\eta_{py}\cot(k_{1z}h) + i\left[i\left(\frac{2\mu+K}{\mu+K}k_y\right)^2 k_{1z} - \frac{\rho_b k_{1z}}{\rho k_{bz}}\frac{\omega^2}{c_2^2}K\eta_{py}\right] \tag{40}$$

$$\Im_{bAp}^{-+} = \left[\frac{(2\mu+K)}{\mu+K}k_y^2 - \frac{\omega^2}{c_2^2}\right] K\eta_{py}\tan(k_{1z}h) - i\left[i\left(\frac{2\mu+K}{\mu+K}k_y\right)^2 k_{1z} - \frac{\rho_b k_{1z}}{\rho k_{bz}}\frac{\omega^2}{c_2^2}K\eta_{py}\right] \tag{41}$$

To determine the transmission coefficient of a plane wave incident on the plate, we employ Equations (21), (22), (32), (33), in conjunction with Equations (19) and (20). The resultant linear system comprising six equations with six unknowns can be expressed in matrix format as :

$$M.x = s, \tag{42}$$

Utilizing Cramer's rule enables us to express the transmission coefficient as follows :

$$T(\omega) = \frac{\Delta_{NT}}{\Delta}, \tag{43}$$

where Δ represents the determinant of M, and Δ_{NT} denotes a determinant of equivalent size achieved by replacing the elements of the first column of Δ with the elements of vector s.

3.2. Numerical study for a polystyrene plate

To observe the outcomes of these theoretical expressions, let's consider an expanded polystyrene (EPS) panel, denoted as such in reference [16], with a thickness of 2cm. This EPS panel is consists of air-filled closed-cell rigid [20] foam (approximately 96% air). The physical properties are detailed in Table 1, where E represents Young's modulus, ν signifies Poisson's ratio, and ρ denotes mass density. The faces of this panel are in contact with air, which has a mass density of 1.29 kg/m^3 and a sound phase velocity of 330 m/s. We represent the modulus of the transmission coefficient, denoted as $|T(\omega)|$, in the frequency and incident angle domain. This information is illustrated in Figure 2 (a) where we could visualize the vibration modes in frequency domain, distinguished by different colors. After that, we have incorporated a hysteretic model to represent the inherent damping characteristics of the panel entails introducing a scalar-valued loss factor into the equation for Young's modulus. This is defined as $E_d(\omega) = E_r(\omega) + iE_i(\omega) = E(\omega)(1 + i\chi(\omega))$, where $E_r(\omega)$ represents the storage modulus and $E_i(\omega)$ indicates the loss modulus of the panel. By employing the specified value of χ, set to 0.06 for EPS as provided in reference [16], the results are depicted in Figure 2 (b), elucidating the absorption properties of the material.

Table 1: Physical properties of the micropolar elastic material.

Material	ρ **(kg/m^3)**	**E (Mpa)**	ν	**K (MPa)**	γ **(MN)**	**J (N/m)**
EPS	12	1.2	0.45	0.037	0.87	3.9×10^{-5}

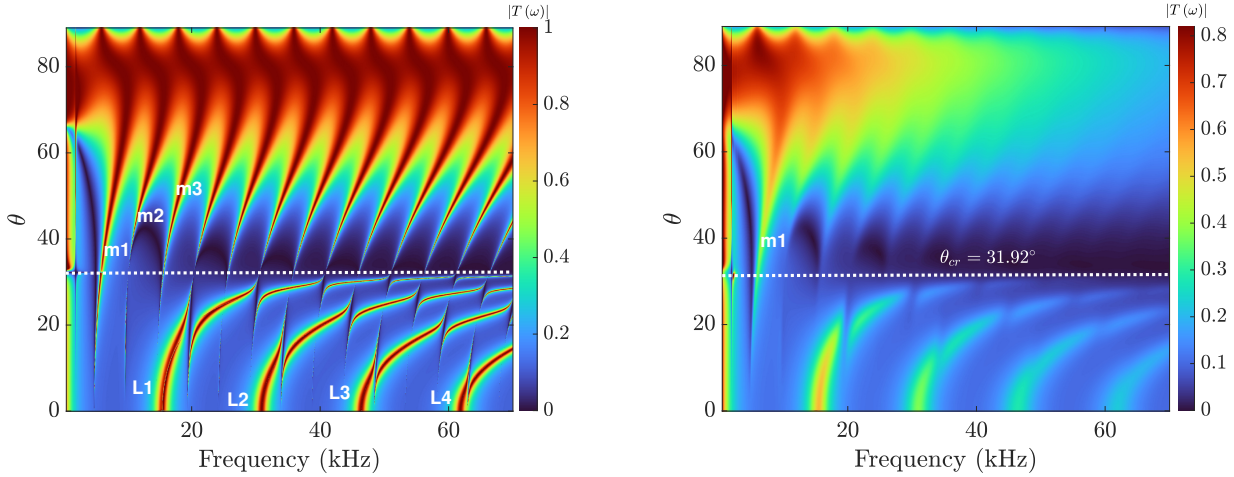

(a) Plate nonabsorbing

(b) Plate absorbing

Figure 2: Theoretical modulus of the transmission coefficient of plate in air, in the frequency-angle of incidence plane

As depicted in both figures, the critical angle delineates an upper limit beyond which the modes L_i ($i = 1,2,3..$) cease to appear. In the region where $\theta < \theta_{cr}$, the behavior of modes L_i ($i = 1,2,3..$) closely resembles that of generalized Lamb waves, hence the designation L (in vacuum, these modes are real and referred to as Lamb modes). Conversely, in the region where $\theta > \theta_{cr}$, the modes m_i ($i = 1,2,3..$) emerge due to the micropolar properties of the material constituting the plate, hence the designation m (for generalized micropolar modes). Both generalized Lamb and micropolar modes indicate that waves propagating in the plate are subject to damping, as some energy escapes from the plate to the surrounding fluid.

4. EXPERIMENTAL METHOD AND SETUP

Figure 3 presents the equipment utilized for signal acquisitions. Initially, a pulse model with a width of 15μs is generated from an Agilent Technologies generator (model 33220A, 20 MHz, Loveland, Colorado, USA) via a Visaton MHT 12 loudspeaker. Signal acquisition involves capturing both the incident signal and transmitted signals at various incidence angles (ranging from 0° to 70° with a 5° increment) using a Brüel & Kjær type 4138-C-006 microphone connected to a National Instruments acquisition system (model PXIe-1090). To enhance signal quality, a Brüel & Kjær type

Figure 3: Experimental setup

2706 power amplifier is inserted between the generator and the loudspeaker, while a Brüel & Kjær type 2121 frequency analyzer is inserted between the microphone and the acquisition system. The modulus of transmission coefficients is derived by calculating the estimated transfer function between the incident acoustic pressure (when there are no samples between the loudspeaker and the microphone) and the pressure obtained with the samples at different angles. This calculation is performed using the tfestimate function in Matlab® with the acquired signals. To minimize spectral leakage and ensure accurate spectral measurements, windowing techniques are initially applied to the temporal signals.

5. RESULTS

Figures 4 (a) and 4 (b) showcase experimental incident and transmitted signals under normal incidence, respectively, in both time and frequency domains. Notably, the signal passing through the panel experiences significant attenuation. Moreover, the transmitted signal precedes the incident signal in the time domain, suggesting a higher wave propagation velocity in the panel compared to air. Additionally, temporal spreading is observed, leading to notable dispersion in the frequency domain. Specifically, the spectrum of the media's response exhibits a substantial reduction in high-frequency components compared to the incident signal, as depicted in Figure 4 (b).

Figure 5 presents a comparison between the modulus of the transmission coefficient in the frequency domain for our plate, utilizing both theoretical and experimental data. Specifically, it compares data for angles below (0° and 5°), where L_i modes are observed, and above (50° and 55°), where m_i modes are observed. Clear observation of L_i and m_i modes is evident, with experimental data closely following the theoretical trend. Resonance frequencies, both theoretical and experimental, generally exhibit close proximity, with better alignment observed for lower incidence angles. Indeed, with the experimental data at normal incidence for exemple, we identified the modes L_1, L_2, and L_3 at frequencies of 17 kHz, 32 kHz, and 50 kHz respectively; and these results are interesting because they predict theoretical results that identify these modes at frequencies of 15.44 kHz, 30.89 kHz, and 46.34 kHz as we can see on Figure 5.

For enhanced visualization and comprehension of vibration mode evolution, a graphical representation was employed, showcasing variations in values across frequency and incidence

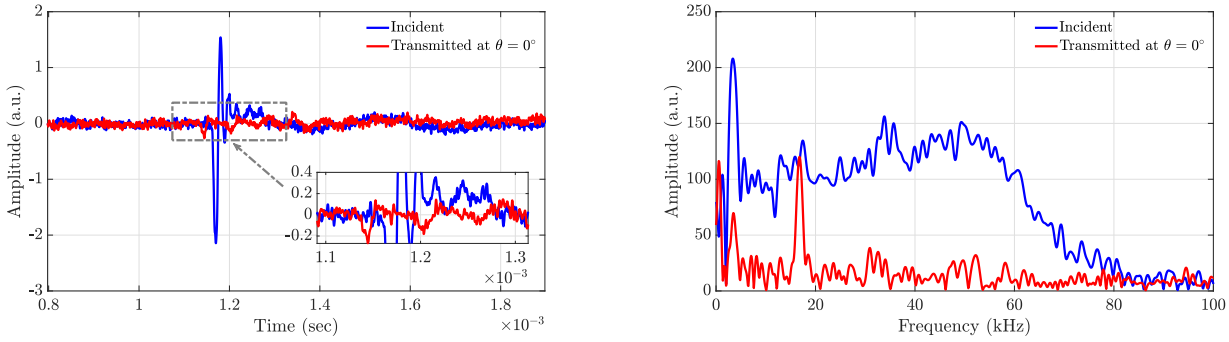

(a) Temporal representation

(b) Frequency spectrum

Figure 4: Illustration of pressure signals representing the incident and transmitted waves.

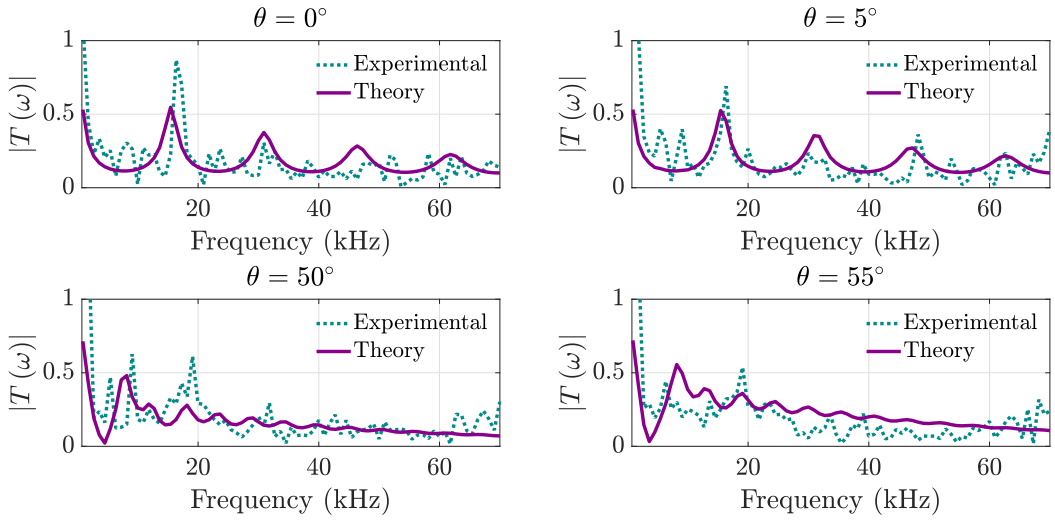

Figure 5: Modulus of the theoretical and experimental transmission coefficient of the 2cm - thick - EPS plate

angle. This presentation, depicted in color on a grid in Figure 6, facilitates insights despite significant attenuation within the media. Notably, the first three L_i modes were discerned.

This graphical approach provides a distinct advantage by accentuating a transitional zone between L_i and m_i modes around critical angles, as theoretically predicted in Section Section 2, specifically 31.92° for the utilized plate. Above θ_{cr} = 31.92°, the first m_1 modes became clearly identifiable. To further elucidate the evolution of L_2 and L_3 modes, we restricted the analysis to specific frequency and angle bands, thereby facilitating improved visualization at an intensified visual scale.

From $T(\omega)$, a complex quantity, we can easily deduce the phase $\Phi(\omega)$, as illustrated in Figure 7. The significance of this phase lies in the fact that it provides us with information about the evolution of the phase velocity, not only in terms of frequency but also in terms of the angle of incidence. Upon observing this data, we first notice a low phase value at the critical angle θ_{cr} across the entire frequency band. Additionally, we observe that for the material used, the wave propagates faster at a frequency of approximately 60 kHz with an angle of incidence of around 10°, as shown in Figure 7, where the maximum value of $\Phi(\omega)$ is reached.

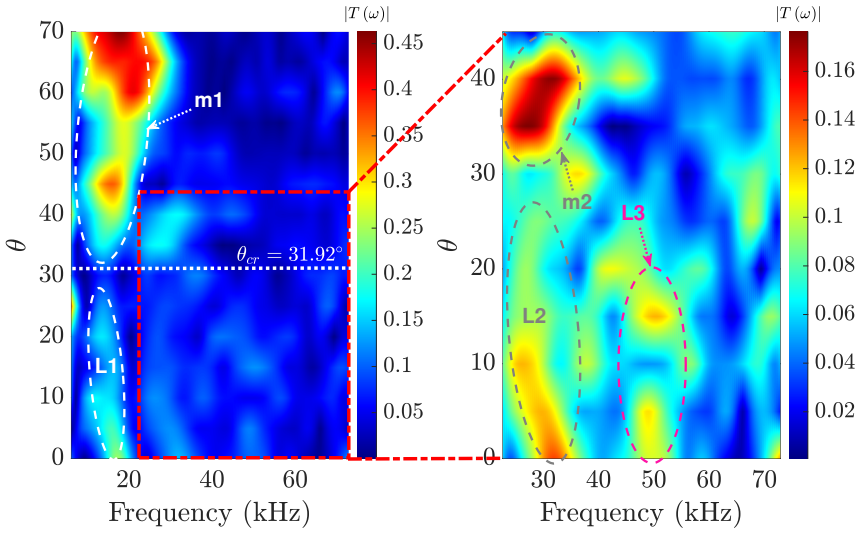

Figure 6: Experimental representation of vibration mode evolution.

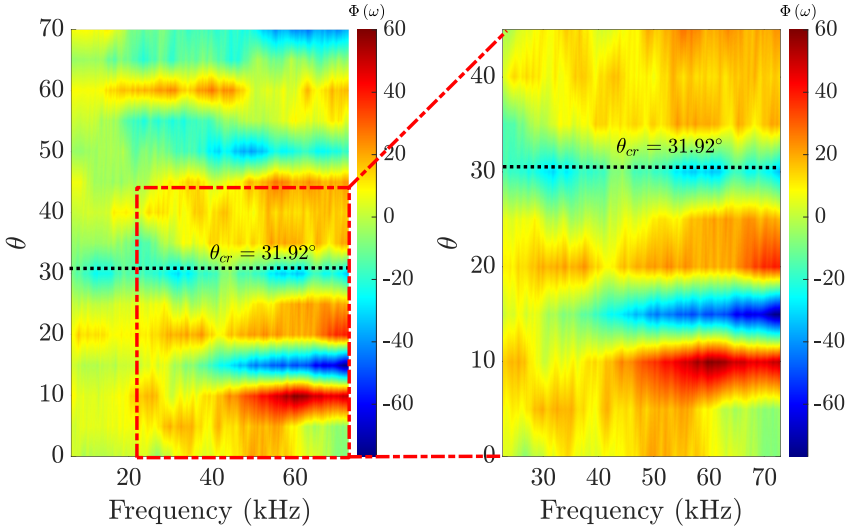

Figure 7: Experimental representation of phase.

6. CONCLUSIONS

In summary, this paper is based on the theory describing the propagation of acoustic waves in a linear and isotropic elastic plate with micropolar behavior, while highlighting the associated vibration modes. To achieve this, we utilized a polystyrene panel whose properties are referenced in [16]. Through an experimental approach using a loudspeaker, a microphone, and a National Instruments data acquisition system, we were able to explore a frequency range from 0 to 70 kHz. This allowed us to identify, starting from normal incidence, at least the first three Lamb modes by observing the modulus of the transmission coefficient, despite the significant attenuation of the medium. We observed that the intensity of these modes decreases in the frequency domain with increasing angle of incidence, reaching a critical transition zone where micropolar modes become observable at angles of incidence greater than the critical angle. These results are consistent with the theoretical predictions presented in the paper. Additionally, graphical analysis of the phase in the frequency and angular domains provides insights into areas of strong medium propagation. Overall, this research offers insights into the properties of these materials commonly employed in industry and construction, especially regarding their role in thermal and acoustic insulation.

ACKNOWLEDGEMENTS

The primary author expresses gratitude to the French Embassy in the Democratic Republic of Congo for their financial support through the "*Bourse du gouvernement français (BGF)*", which enabled this research. Appreciation is also extended to the Polytechnic Faculty of the University of Kinshasa for their assistance in training. Lastly, the authors acknowledge the valuable contributions of the anonymous reviewers from *INTER-NOISE 2024 NANTES FRANCE* for their critiques and recommendations.

REFERENCES

1. Eugène Maurice Pierre Cosserat and François Cosserat. *Théorie des corps déformables*. A. Hermann et fils, 1909.
2. RA144512 Toupin. Elastic materials with couple-stresses. *Archive for rational mechanics and analysis*, 11(1):385–414, 1962.
3. Raymond David Mindlin, HF144513 Tiersten, et al. Effects of couple-stresses in linear elasticity. *Archive for Rational Mechanics and analysis*, 11(1):415–448, 1962.
4. RD Mindlin. Stress functions for a cosserat continuum. *International Journal of Solids and Structures*, 1(3):265–271, 1965.
5. WT163469 Koiter. Couple-stresses in the theory of elasticity, i & ii. 1969.
6. Gérard A Maugin and Andrei V Metrikine. Mechanics of generalized continua. 2010.
7. A Cemal Eringen and A Cemal Eringen. *Theory of micropolar elasticity*. Springer, 1999.
8. A Cemal Eringen. Linear theory of micropolar elasticity. *Journal of Mathematics and Mechanics*, pages 909–923, 1966.
9. A Cemal Eringen. *Microcontinuum field theories: I. Foundations and solids*. Springer Science & Business Media, 2012.
10. CB Kafadar and A Cemal Eringen. Micropolar media—i the classical theory. *International Journal of Engineering Science*, 9(3):271–305, 1971.
11. Soroosh Hassanpour and Glenn R Heppler. Micropolar elasticity theory: a survey of linear isotropic equations, representative notations, and experimental investigations. *Mathematics and Mechanics of Solids*, 22(2):224–242, 2017.
12. Igor Aleksandrovich Viktorov. Rayleigh and lamb waves. *Rayleigh and Lamb Waves*, page 33, 1967.
13. Ralph Fiorito, Walter Madigosky, and Herbert Überall. Resonance theory of acoustic waves interacting with an elastic plate. *The Journal of the Acoustical Society of America*, 66(6):1857–1866, 1979.
14. Herbert Überall. Surface waves in acoustics. In *Physical acoustics*, volume 10, pages 1–60. Elsevier, 1973.
15. H Franklin, E Danila, and J-M Conoir. S-matrix theory applied to acoustic scattering by asymmetrically fluid-loaded elastic isotropic plates. *The Journal of the Acoustical Society of America*, 110(1):243–253, 2001.
16. Erick Ogam, Zine El Abbidine Fellah, Mohamed Fellah, and Claude Depollier. Theoretical and experimental study of micropolar elastic materials using acoustic waves in air. *Journal of Sound and Vibration*, 510:116298, 2021.
17. VAUGHN RUPERT Parfitt and AC Eringen. Reflection of plane waves from the flat boundary of a micropolar elastic half-space. *The Journal of the Acoustical Society of America*, 45(5):1258–1272, 1969.
18. Dilbag Singh and SK Tomar. Longitudinal waves at a micropolar fluid/solid interface. *International Journal of Solids and Structures*, 45(1):225–244, 2008.

19. Julius Miklowitz. Elastic waves and waveguides. 1978.
20. Michael F Ashby and Lorna J Gibson. Cellular solids: structure and properties. *Press Syndicate of the University of Cambridge, Cambridge, UK*, pages 175–231, 1997.